

12-2017

Search for light tetraquark states in $\Upsilon (1 S)$ and $\Upsilon (2 S)$ decays

S. Jia et al.

Belle Collaboration

David Joffe

Kennesaw State University, djoffe@kennesaw.edu

Ratnappuli L. Kulasiri

Kennesaw State University, rkulasir@kennesaw.edu

Follow this and additional works at: <https://digitalcommons.kennesaw.edu/facpubs>



Part of the [Physics Commons](#)

Recommended Citation

et al., S. Jia; Joffe, David; and Kulasiri, Ratnappuli L., "Search for light tetraquark states in $\Upsilon (1 S)$ and $\Upsilon (2 S)$ decays" (2017).

Faculty Publications. 4172.

<https://digitalcommons.kennesaw.edu/facpubs/4172>

Search for light tetraquark states in $\Upsilon(1S)$ and $\Upsilon(2S)$ decays

S. Jia,² C. P. Shen,² C. Z. Yuan,²⁵ I. Adachi,^{16,12} J. K. Ahn,³⁹ H. Aihara,⁸² S. Al Said,^{76,37}
 D. M. Asner,⁶⁴ H. Atmacan,⁷² T. Aushev,⁵² R. Ayad,⁷⁶ V. Babu,⁷⁷ I. Badhrees,^{76,36}
 S. Bahinipati,²⁰ A. M. Bakich,⁷⁵ V. Bansal,⁶⁴ P. Behera,²³ M. Berger,⁷³ V. Bhardwaj,¹⁹
 B. Bhuyan,²¹ J. Biswal,³² G. Bonvicini,⁸⁷ A. Bozek,⁵⁹ M. Bračko,^{47,32} T. E. Browder,¹⁵
 D. Červenkov,⁴ M.-C. Chang,⁹ V. Chekelian,⁴⁸ A. Chen,⁵⁶ B. G. Cheon,¹⁴ K. Chilikin,^{43,51}
 K. Cho,³⁸ S.-K. Choi,¹³ Y. Choi,⁷⁴ D. Cinabro,⁸⁷ T. Czank,⁸⁰ N. Dash,²⁰ S. Di Carlo,⁸⁷
 Z. Doležal,⁴ D. Dutta,⁷⁷ S. Eidelman,^{3,62} D. Epifanov,^{3,62} J. E. Fast,⁶⁴ T. Ferber,⁷ B. G. Fulsom,⁶⁴
 R. Garg,⁶⁵ V. Gaur,⁸⁶ N. Gabyshev,^{3,62} A. Garmash,^{3,62} M. Gelb,³⁴ A. Giri,²² P. Goldenzweig,³⁴
 O. Grzymkowska,⁵⁹ E. Guido,³⁰ J. Haba,^{16,12} T. Hara,^{16,12} K. Hayasaka,⁶¹ H. Hayashii,⁵⁵
 M. T. Hedges,¹⁵ W.-S. Hou,⁵⁸ T. Iijima,^{54,53} K. Inami,⁵³ G. Inguglia,⁷ A. Ishikawa,⁸⁰ R. Itoh,^{16,12}
 M. Iwasaki,⁶³ Y. Iwasaki,¹⁶ W. W. Jacobs,²⁴ I. Jaegle,⁸ Y. Jin,⁸² D. Joffe,³⁵ K. K. Joo,⁵ T. Julius,⁴⁹
 A. B. Kaliyar,²³ G. Karyan,⁷ T. Kawasaki,⁶¹ H. Kichimi,¹⁶ C. Kiesling,⁴⁸ D. Y. Kim,⁷¹
 H. J. Kim,⁴¹ J. B. Kim,³⁹ K. T. Kim,³⁹ S. H. Kim,¹⁴ P. Kodyš,⁴ S. Korpar,^{47,32} D. Kotchetkov,¹⁵
 P. Križan,^{44,32} R. Kroeger,²⁸ P. Krokovny,^{3,62} R. Kulasiri,³⁵ T. Kumita,⁸⁴ A. Kuzmin,^{3,62}
 Y.-J. Kwon,⁸⁹ J. S. Lange,¹⁰ I. S. Lee,¹⁴ S. C. Lee,⁴¹ L. K. Li,²⁵ Y. Li,⁸⁶ L. Li Gioi,⁴⁸ J. Libby,²³
 D. Liventsev,^{86,16} M. Lubej,³² T. Luo,⁶⁶ M. Masuda,⁸¹ T. Matsuda,⁵⁰ D. Matvienko,^{3,62}
 M. Merola,²⁹ K. Miyabayashi,⁵⁵ H. Miyata,⁶¹ R. Mizuk,^{43,51,52} H. K. Moon,³⁹ T. Mori,⁵³
 R. Mussa,³⁰ M. Nakao,^{16,12} T. Nanut,³² K. J. Nath,²¹ Z. Natkaniec,⁵⁹ M. Nayak,^{87,16}
 M. Niiyama,⁴⁰ N. K. Nisar,⁶⁶ S. Nishida,^{16,12} S. Ogawa,⁷⁹ S. Okuno,³³ S. L. Olsen,⁶⁹ H. Ono,^{60,61}
 Y. Onuki,⁸² P. Pakhlov,^{43,51} G. Pakhlova,^{43,52} B. Pal,⁶ S. Pardi,²⁹ C. W. Park,⁷⁴ H. Park,⁴¹
 S. Paul,⁷⁸ I. Pavelkin,⁵² R. Pestotnik,³² L. E. Piilonen,⁸⁶ M. Ritter,⁴⁵ A. Rostomyan,⁷
 G. Russo,²⁹ Y. Sakai,^{16,12} M. Salehi,^{46,45} S. Sandilya,⁶ L. Santelj,¹⁶ T. Sanuki,⁸⁰ V. Savinov,⁶⁶
 O. Schneider,⁴² G. Schnell,^{1,18} C. Schwanda,²⁶ Y. Seino,⁶¹ K. Senyo,⁸⁸ O. Seon,⁵³ M. E. Seviar,⁴⁹
 V. Shebalin,^{3,62} T.-A. Shibata,⁸³ N. Shimizu,⁸² J.-G. Shiu,⁵⁸ B. Shwartz,^{3,62} J. B. Singh,⁶⁵
 A. Sokolov,²⁷ E. Solovieva,^{43,52} M. Starič,³² J. Stypula,⁵⁹ M. Sumihama,¹¹ T. Sumiyoshi,⁸⁴
 M. Takizawa,^{70,17,67} U. Tamponi,^{30,85} K. Tanida,³¹ F. Tenchini,⁴⁹ M. Uchida,⁸³ T. Uglov,^{43,52}
 Y. Unno,¹⁴ S. Uno,^{16,12} P. Urquijo,⁴⁹ Y. Usov,^{3,62} C. Van Hulse,¹ G. Varner,¹⁵ A. Vossen,²⁴
 B. Wang,⁶ C. H. Wang,⁵⁷ M.-Z. Wang,⁵⁸ P. Wang,²⁵ X. L. Wang,^{64,16} M. Watanabe,⁶¹
 Y. Watanabe,³³ E. Widmann,⁷³ E. Won,³⁹ Y. Yamashita,⁶⁰ H. Ye,⁷ Y. Yusa,⁶¹ S. Zakharov,⁴³
 Z. P. Zhang,⁶⁸ V. Zhilich,^{3,62} V. Zhukova,^{43,51} V. Zhulanov,^{3,62} and A. Zupanc^{44,32}

(The Belle Collaboration)

¹University of the Basque Country UPV/EHU, 48080 Bilbao

²Beihang University, Beijing 100191

³Budker Institute of Nuclear Physics SB RAS, Novosibirsk 630090

⁴Faculty of Mathematics and Physics, Charles University, 121 16 Prague

⁵Chonnam National University, Kwangju 660-701

⁶University of Cincinnati, Cincinnati, Ohio 45221

⁷Deutsches Elektronen-Synchrotron, 22607 Hamburg

⁸University of Florida, Gainesville, Florida 32611

⁹Department of Physics, Fu Jen Catholic University, Taipei 24205

- ¹⁰*Justus-Liebig-Universität Gießen, 35392 Gießen*
- ¹¹*Gifu University, Gifu 501-1193*
- ¹²*SOKENDAI (The Graduate University for Advanced Studies), Hayama 240-0193*
- ¹³*Gyeongsang National University, Chinju 660-701*
- ¹⁴*Hanyang University, Seoul 133-791*
- ¹⁵*University of Hawaii, Honolulu, Hawaii 96822*
- ¹⁶*High Energy Accelerator Research Organization (KEK), Tsukuba 305-0801*
- ¹⁷*J-PARC Branch, KEK Theory Center,
High Energy Accelerator Research Organization (KEK), Tsukuba 305-0801*
- ¹⁸*IKERBASQUE, Basque Foundation for Science, 48013 Bilbao*
- ¹⁹*Indian Institute of Science Education and Research Mohali, SAS Nagar, 140306*
- ²⁰*Indian Institute of Technology Bhubaneswar, Satya Nagar 751007*
- ²¹*Indian Institute of Technology Guwahati, Assam 781039*
- ²²*Indian Institute of Technology Hyderabad, Telangana 502285*
- ²³*Indian Institute of Technology Madras, Chennai 600036*
- ²⁴*Indiana University, Bloomington, Indiana 47408*
- ²⁵*Institute of High Energy Physics, Chinese Academy of Sciences, Beijing 100049*
- ²⁶*Institute of High Energy Physics, Vienna 1050*
- ²⁷*Institute for High Energy Physics, Protvino 142281*
- ²⁸*University of Mississippi, University, Mississippi 38677*
- ²⁹*INFN - Sezione di Napoli, 80126 Napoli*
- ³⁰*INFN - Sezione di Torino, 10125 Torino*
- ³¹*Advanced Science Research Center, Japan Atomic Energy Agency, Naka 319-1195*
- ³²*J. Stefan Institute, 1000 Ljubljana*
- ³³*Kanagawa University, Yokohama 221-8686*
- ³⁴*Institut für Experimentelle Kernphysik,
Karlsruher Institut für Technologie, 76131 Karlsruhe*
- ³⁵*Kennesaw State University, Kennesaw, Georgia 30144*
- ³⁶*King Abdulaziz City for Science and Technology, Riyadh 11442*
- ³⁷*Department of Physics, Faculty of Science,
King Abdulaziz University, Jeddah 21589*
- ³⁸*Korea Institute of Science and Technology Information, Daejeon 305-806*
- ³⁹*Korea University, Seoul 136-713*
- ⁴⁰*Kyoto University, Kyoto 606-8502*
- ⁴¹*Kyungpook National University, Daegu 702-701*
- ⁴²*École Polytechnique Fédérale de Lausanne (EPFL), Lausanne 1015*

⁴³*P.N. Lebedev Physical Institute of the Russian Academy of Sciences, Moscow 119991*

⁴⁴*Faculty of Mathematics and Physics,
University of Ljubljana, 1000 Ljubljana*

⁴⁵*Ludwig Maximilians University, 80539 Munich*

⁴⁶*University of Malaya, 50603 Kuala Lumpur*

⁴⁷*University of Maribor, 2000 Maribor*

⁴⁸*Max-Planck-Institut für Physik, 80805 München*

⁴⁹*School of Physics, University of Melbourne, Victoria 3010*

⁵⁰*University of Miyazaki, Miyazaki 889-2192*

⁵¹*Moscow Physical Engineering Institute, Moscow 115409*

⁵²*Moscow Institute of Physics and Technology, Moscow Region 141700*

⁵³*Graduate School of Science, Nagoya University, Nagoya 464-8602*

⁵⁴*Kobayashi-Maskawa Institute, Nagoya University, Nagoya 464-8602*

⁵⁵*Nara Women's University, Nara 630-8506*

⁵⁶*National Central University, Chung-li 32054*

⁵⁷*National United University, Miao Li 36003*

⁵⁸*Department of Physics, National Taiwan University, Taipei 10617*

⁵⁹*H. Niewodniczanski Institute of Nuclear Physics, Krakow 31-342*

⁶⁰*Nippon Dental University, Niigata 951-8580*

⁶¹*Niigata University, Niigata 950-2181*

⁶²*Novosibirsk State University, Novosibirsk 630090*

⁶³*Osaka City University, Osaka 558-8585*

⁶⁴*Pacific Northwest National Laboratory, Richland, Washington 99352*

⁶⁵*Panjab University, Chandigarh 160014*

⁶⁶*University of Pittsburgh, Pittsburgh, Pennsylvania 15260*

⁶⁷*Theoretical Research Division, Nishina Center, RIKEN, Saitama 351-0198*

⁶⁸*University of Science and Technology of China, Hefei 230026*

⁶⁹*Seoul National University, Seoul 151-742*

⁷⁰*Showa Pharmaceutical University, Tokyo 194-8543*

⁷¹*Soongsil University, Seoul 156-743*

⁷²*University of South Carolina, Columbia, South Carolina 29208*

⁷³*Stefan Meyer Institute for Subatomic Physics, Vienna 1090*

⁷⁴*Sungkyunkwan University, Suwon 440-746*

⁷⁵*School of Physics, University of Sydney, New South Wales 2006*

⁷⁶*Department of Physics, Faculty of Science, University of Tabuk, Tabuk 71451*

⁷⁷*Tata Institute of Fundamental Research, Mumbai 400005*

⁷⁸*Department of Physics, Technische Universität München, 85748 Garching*

⁷⁹*Toho University, Funabashi 274-8510*

⁸⁰*Department of Physics, Tohoku University, Sendai 980-8578*

⁸¹*Earthquake Research Institute, University of Tokyo, Tokyo 113-0032*

⁸²*Department of Physics, University of Tokyo, Tokyo 113-0033*

⁸³*Tokyo Institute of Technology, Tokyo 152-8550*

⁸⁴*Tokyo Metropolitan University, Tokyo 192-0397*

⁸⁵*University of Torino, 10124 Torino*

⁸⁶*Virginia Polytechnic Institute and State University, Blacksburg, Virginia 24061*

⁸⁷*Wayne State University, Detroit, Michigan 48202*

⁸⁸*Yamagata University, Yamagata 990-8560*

⁸⁹*Yonsei University, Seoul 120-749*

Abstract

We search for the $J^{PC} = 0^{--}$ and 1^{+-} light tetraquark states with masses up to $2.46 \text{ GeV}/c^2$ in $\Upsilon(1S)$ and $\Upsilon(2S)$ decays with data samples of (102 ± 2) million and (158 ± 4) million events, respectively, collected with the Belle detector. No significant signals are observed in any of the studied production modes, and 90% credibility level (C.L.) upper limits on their branching fractions in $\Upsilon(1S)$ and $\Upsilon(2S)$ decays are obtained. The inclusive branching fractions of the $\Upsilon(1S)$ and $\Upsilon(2S)$ decays into final states with $f_1(1285)$ are measured to be $\mathcal{B}(\Upsilon(1S) \rightarrow f_1(1285) + \textit{anything}) = (46 \pm 28(\text{stat.}) \pm 13(\text{syst.})) \times 10^{-4}$ and $\mathcal{B}(\Upsilon(2S) \rightarrow f_1(1285) + \textit{anything}) = (22 \pm 15(\text{stat.}) \pm 6.3(\text{syst.})) \times 10^{-4}$. The measured $\chi_{b2} \rightarrow J/\psi + \textit{anything}$ branching fraction is measured to be $(1.50 \pm 0.34(\text{stat.}) \pm 0.22(\text{syst.})) \times 10^{-3}$, and 90% C.L. upper limits for the $\chi_{b0,b1} \rightarrow J/\psi + \textit{anything}$ branching fractions are found to be 2.3×10^{-3} and 1.1×10^{-3} , respectively. For $\mathcal{B}(\chi_{b1} \rightarrow \omega + \textit{anything})$, the branching fraction is measured to be $(4.9 \pm 1.3(\text{stat.}) \pm 0.6(\text{syst.})) \times 10^{-2}$. All results reported here are the first measurements for these modes.

PACS numbers: 14.40.Rt, 13.30.Eg, 13.20.Gd

I. INTRODUCTION

In the past decade, many experiments, both at lepton and hadron colliders, have reported evidence for a large number of particles having properties that can not be readily explained within the framework of the expected heavy quarkonium states [1, 2]. Among them, the $X(3872)$ [3], the $Z_c(3900)$ [4, 5], the $X(3940)$ [6], the $Y(4260)$ [7, 8], the $Z(4430)$ [9], the $Z_b(10610)$ and the $Z_b(10650)$ [10], are generally interpreted as possible tetraquark candidates with exotic properties.

In the low-mass region, the Dalitz analysis of the decay $D^0 \rightarrow \pi^+\pi^-\pi^0$ [11] indicates the existence of a state decaying into a $\rho\pi$ final state with exotic quantum numbers $J^{PC} = 0^{--}$ [12] at a mass of $\approx 1865 \text{ MeV}/c^2$, which cannot be composed of a quark-antiquark pair in the conventional quark model [13, 14]. If such a resonance exists, it might be a hybrid or a tetraquark state [15].

The authors of Ref. [16] calculated the masses of such exotic four-quark states with $J^{PC} = 0^{--}$ and 1^{+-} in Laplace sum rules (LSR) and finite-energy sum rules (FESR) using tetraquark-like currents. In the scalar channel, both LSR and FESR gave consistent mass predictions of a tetraquark state with a mass of $(1.66 \pm 0.14) \text{ GeV}/c^2$. This numerical result favors the tetraquark interpretation of the possible $\rho\pi$ dominance in the D^0 decays. In the vector channel, the authors also conservatively estimated the mass of a tetraquark state to be in the mass region $1.18 - 1.43 \text{ GeV}/c^2$. Although the masses have been calculated, the width and couplings to any final states were not predicted.

Very recently, the Belle Collaboration reported the search for the $J^{PC} = 0^{--}$ glueball ($G_{0^{--}}$) in the production modes $\Upsilon(1S, 2S) \rightarrow \chi_{c1} + G_{0^{--}}$, $\Upsilon(1S, 2S) \rightarrow f_1(1285) + G_{0^{--}}$, $\chi_{b1} \rightarrow J/\psi + G_{0^{--}}$, and $\chi_{b1} \rightarrow \omega + G_{0^{--}}$ with data samples of (102 ± 2) million $\Upsilon(1S)$ and (158 ± 4) million $\Upsilon(2S)$ events [17]. The masses of the putative glueballs were fixed at 2.800, 3.810, and 4.330 $\text{ GeV}/c^2$, as predicted from quantum chromodynamics (QCD) sum rules [18] and distinct bottom-up holographic models of QCD [19]. Considering the kinematical constraints and the conservation of the quantum numbers J^{PC} , the production modes for glueball searches are also suitable for searches for the aforementioned light tetraquark states with $J^{PC} = 0^{--}$ and 1^{+-} , denoted collectively as X_{tetra} .

In this paper, we utilize the low-mass recoil spectra of the χ_{c1} , $f_1(1285)$, J/ψ , and ω in bottomonium decays to search for X_{tetra} signals in the modes $\Upsilon(1S, 2S) \rightarrow \chi_{c1} + X_{\text{tetra}}$, $\Upsilon(1S, 2S) \rightarrow f_1(1285) + X_{\text{tetra}}$, $\chi_{b1} \rightarrow J/\psi + X_{\text{tetra}}$, and $\chi_{b1} \rightarrow \omega + X_{\text{tetra}}$ [17]. Since the X_{tetra} properties are unknown, we report our investigation for different assumed values for the X_{tetra} mass and width.

As byproducts of the X_{tetra} search, we measure the inclusive $f_1(1285)$ production in $\Upsilon(1S, 2S)$, J/ψ production in $\chi_{bJ}(J = 0, 1, 2)$, and ω production in χ_{b1} decays.

II. THE DATA SAMPLE AND BELLE DETECTOR

This analysis utilizes the Belle $\Upsilon(1S)$ and $\Upsilon(2S)$ data samples with a total luminosity of 5.74 and 24.91 fb^{-1} , respectively, corresponding to $(102 \pm 2) \times 10^6$ $\Upsilon(1S)$ and $(158 \pm 4) \times 10^6$ $\Upsilon(2S)$ events [20]. An 89.45 fb^{-1} data sample collected at $\sqrt{s} = 10.52 \text{ GeV}$ is used to estimate the possible irreducible contributions from continuum ($e^+e^- \rightarrow q\bar{q}$, where $q \in \{u, d, s, c\}$). Here, \sqrt{s} is the center-of-mass (C.M.) energy of the colliding e^+e^- system. The data were collected with the Belle detector [21, 22] operated at the KEKB asymmetric-energy e^+e^- collider [23, 24]. Large

Monte Carlo (MC) samples of all of the investigated tetraquark modes are generated with EVTGEN [25] and simulated with a GEANT3-based [26] model for the detector response to determine the signal line-shapes and efficiencies. The angular distribution for the decay $\Upsilon(2S) \rightarrow \gamma\chi_{bJ}$ is simulated assuming a pure E1 transition ($dN/d\cos\theta_\gamma \propto 1 + \alpha\cos^2\theta_\gamma$ with $\alpha = 1, -\frac{1}{3}, \frac{1}{13}$ for $J = 0, 1, 2$, respectively [27], where θ_γ is the polar angle of the $\Upsilon(2S)$ radiative photon in the e^+e^- C.M. frame); a phase space model in EVTGEN is used for the χ_{bJ} decays. We use the phase space model for other decays as well. Note that the X_{tetra} inclusive decays are modelled using PYTHIA [28]. Inclusive $\Upsilon(1S)$ and $\Upsilon(2S)$ MC samples, produced using PYTHIA with four times the total numbers of $\Upsilon(1S, 2S)$ events of the data, are used to identify possible backgrounds showing peak distributions from $\Upsilon(1S)$ and $\Upsilon(2S)$ decays.

The Belle detector is a large solid-angle magnetic spectrometer that consists of a silicon vertex detector, a 50-layer central drift chamber, an array of aerogel threshold Cherenkov counters, a barrel-like arrangement of time-of-flight scintillation counters, and an electromagnetic calorimeter comprised of CsI(Tl) crystals located inside a superconducting solenoid coil that provides a 1.5 T magnetic field. An iron flux-return yoke instrumented with resistive plate chambers located outside the coil is used to detect K_L^0 mesons and to identify muons. A detailed description of the Belle detector can be found in Refs. [21, 22].

III. MEASUREMENTS OF $\Upsilon(1S, 2S) \rightarrow f_1(1285) + \text{anything}$

Candidate $f_1(1285)$ states are reconstructed via $\eta\pi^+\pi^-$, $\eta \rightarrow \gamma\gamma$. Considering the differences in the MC-determined reconstruction efficiencies for different $f_1(1285)$ momenta, we partition the data samples according to the scaled momentum $x = 2\sqrt{s} \times p_{f_1(1285)}^*/(s - m_{f_1(1285)}^2)$, where $p_{f_1(1285)}^*$ is the momentum of the $f_1(1285)$ candidate in the C.M. system, and $m_{f_1(1285)}$ is the $f_1(1285)$ nominal mass [13]. The normalizing expression $(s - m_{f_1(1285)}^2)/(2\sqrt{s})$ represents the maximum value of $p_{f_1(1285)}^*$ for the case where the $f_1(1285)$ candidate recoils against a massless particle. The use of x removes the beam-energy dependence in comparing the continuum data to those taken at the $\Upsilon(1S, 2S)$ resonances. The event selections are identical to those used in Ref. [17]. Figure 1 shows the reconstruction efficiencies as a function of x for $f_1(1285)$ candidates from $\Upsilon(1S, 2S)$ decays in each x interval. Here, the efficiencies are estimated using a MC signal sample generated on the basis of the relative weights of the differential branching fractions (discussed below) in the different x bins.

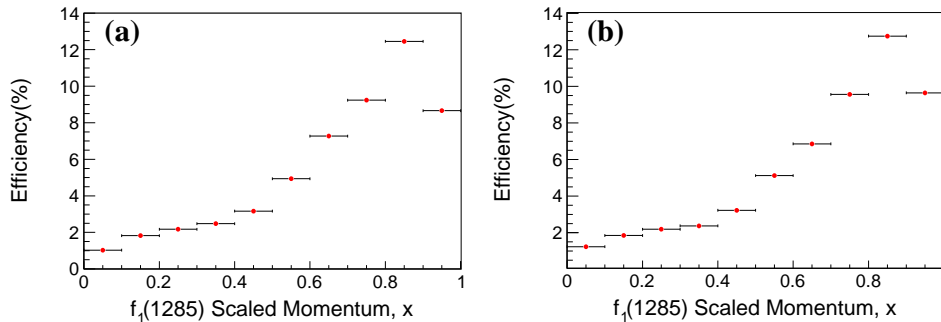


FIG. 1: MC efficiencies for reconstructed $f_1(1285)$ mesons in (a) $\Upsilon(1S)$ and (b) $\Upsilon(2S)$ decays as a function of the scaled momentum x .

The invariant mass distributions for the $f_1(1285)$ candidates in $\Upsilon(1S, 2S)$ data for the entire x

TABLE I: Summary of the branching fraction measurements of $\Upsilon(1S, 2S)$ inclusive decays into $f_1(1285)$, where N_{fit} is the number of fitted signal events, ε is the reconstruction efficiency, σ_{syst} is the relative total systematic uncertainty, and \mathcal{B} is the measured branching fraction.

x	$\Upsilon(1S) \rightarrow f_1(1285) + \text{anything}$				$\Upsilon(2S) \rightarrow f_1(1285) + \text{anything}$			
	N_{fit}	$\varepsilon(\%)$	$\sigma_{\text{syst}}(\%)$	$\mathcal{B}(10^{-4})$	N_{fit}	$\varepsilon(\%)$	$\sigma_{\text{syst}}(\%)$	$\mathcal{B}(10^{-4})$
(0.0, 0.1)	-480 ± 239	1.03	24.5	$-32 \pm 16 \pm 8.0$	-442 ± 253	1.23	29.8	$-16 \pm 9.2 \pm 4.8$
(0.1, 0.2)	727 ± 497	1.82	25.5	$28 \pm 19 \pm 7.1$	265 ± 192	1.85	26.9	$6.4 \pm 4.7 \pm 1.8$
(0.2, 0.3)	-432 ± 339	2.17	24.6	$-14 \pm 11 \pm 3.4$	-749 ± 333	2.19	26.0	$-15 \pm 6.8 \pm 4.0$
(0.3, 0.4)	1181 ± 240	2.48	28.9	$33 \pm 6.7 \pm 9.6$	1296 ± 348	2.37	25.3	$24 \pm 6.6 \pm 6.2$
(0.4, 0.5)	736 ± 165	3.16	24.2	$16 \pm 3.6 \pm 3.9$	801 ± 247	3.22	26.7	$11 \pm 3.5 \pm 3.0$
(0.5, 0.6)	645 ± 126	4.94	36.4	$9.0 \pm 1.8 \pm 3.3$	590 ± 189	5.12	34.9	$5.1 \pm 1.7 \pm 1.8$
(0.6, 0.7)	412 ± 88	7.27	31.3	$3.9 \pm 0.9 \pm 1.3$	563 ± 143	6.86	32.6	$3.7 \pm 1.0 \pm 1.2$
(0.7, 0.8)	229 ± 65	9.24	42.8	$1.7 \pm 0.5 \pm 0.8$	382 ± 70	9.56	35.6	$1.8 \pm 0.4 \pm 0.7$
(0.8, 0.9)	66 ± 38	12.46	48.0	$0.4 \pm 0.3 \pm 0.2$	205 ± 84	12.75	36.3	$0.7 \pm 0.3 \pm 0.3$
(0.9, 1.0)	16 ± 11	8.66	55.0	$0.1 \pm 0.1 \pm 0.1$	15 ± 11	9.65	48.9	$0.1 \pm 0.1 \pm 0.1$
All x	3100 ± 950	4.68	28.7	$46 \pm 28 \pm 13$	2926 ± 712	5.93	28.4	$22 \pm 15 \pm 6.3$

region and for subranges in x are shown in Figs. 2 and 3. We observe clear $f_1(1285)$ signals in high- x bins and $\eta(1405)$ signals in the subregion $0.6 < x < 1.0$. In the figures, the cross-hatched histograms are from the normalized continuum contributions. See Ref. [17] for the definition of the normalization method of the continuum contribution. For $\Upsilon(2S) \rightarrow f_1(1285) + \text{anything}$, a further background arises from the intermediate transition $\Upsilon(2S) \rightarrow \pi^+\pi^-\Upsilon(1S)$ or $\pi^0\pi^0\Upsilon(1S)$ with $\Upsilon(1S)$ decaying to $f_1(1285)$. This contamination is removed by requiring the $\pi\pi$ recoil mass to be outside the $[9.45, 9.47]$ GeV/ c^2 range for all $\pi\pi$ combinations [17].

A binned extended simultaneous likelihood fit is applied to the x -dependent $\eta\pi^+\pi^-$ invariant mass spectra to extract the $f_1(1285)$ signal yields in the $\Upsilon(1S, 2S)$ and continuum data samples. Due to the dependence on momentum, the $f_1(1285)$ and $\eta(1405)$ signal shapes in each x bin are described by Voigtian functions (a Breit-Wigner distribution convolved with a Gaussian function) that are obtained from the MC simulations directly; a third-order Chebyshev polynomial background shape is used for the $\Upsilon(1S, 2S)$ decay backgrounds in addition to the normalized continuum contributions. The fit results are shown in Figs. 2 and 3 for the $\Upsilon(1S)$ and $\Upsilon(2S)$ decays, respectively. The fitted $f_1(1285)$ signal yields (N_{fit}) in each x bin from $\Upsilon(1S)$ and $\Upsilon(2S)$ decays are tabulated in Table I, together with the reconstruction efficiencies from MC signal simulations (ε), the total systematic uncertainties (σ_{syst}) discussed below (which are the sum of the common systematic errors, fit uncertainties and continuum-scale-factor uncertainties), and the corresponding branching fractions (\mathcal{B}). The total numbers of $f_1(1285)$ events, *i.e.*, the sums of the signal yields in all of the x bins, the sums of the x -dependent efficiencies weighted by the signal fraction in that x bin, and the measured branching fractions are listed in the bottom row of Table I. The branching fractions for $\Upsilon(1S, 2S) \rightarrow f_1(1285) + \text{anything}$ are measured to be:

$$\mathcal{B}(\Upsilon(1S) \rightarrow f_1(1285) + \text{anything}) = (46 \pm 28(\text{stat.}) \pm 13(\text{syst.})) \times 10^{-4},$$

$$\mathcal{B}(\Upsilon(2S) \rightarrow f_1(1285) + \text{anything}) = (22 \pm 15(\text{stat.}) \pm 6.3(\text{syst.})) \times 10^{-4}.$$

The differential branching fractions of $\Upsilon(1S, 2S)$ decays to $f_1(1285)$ are shown in Fig. 4.

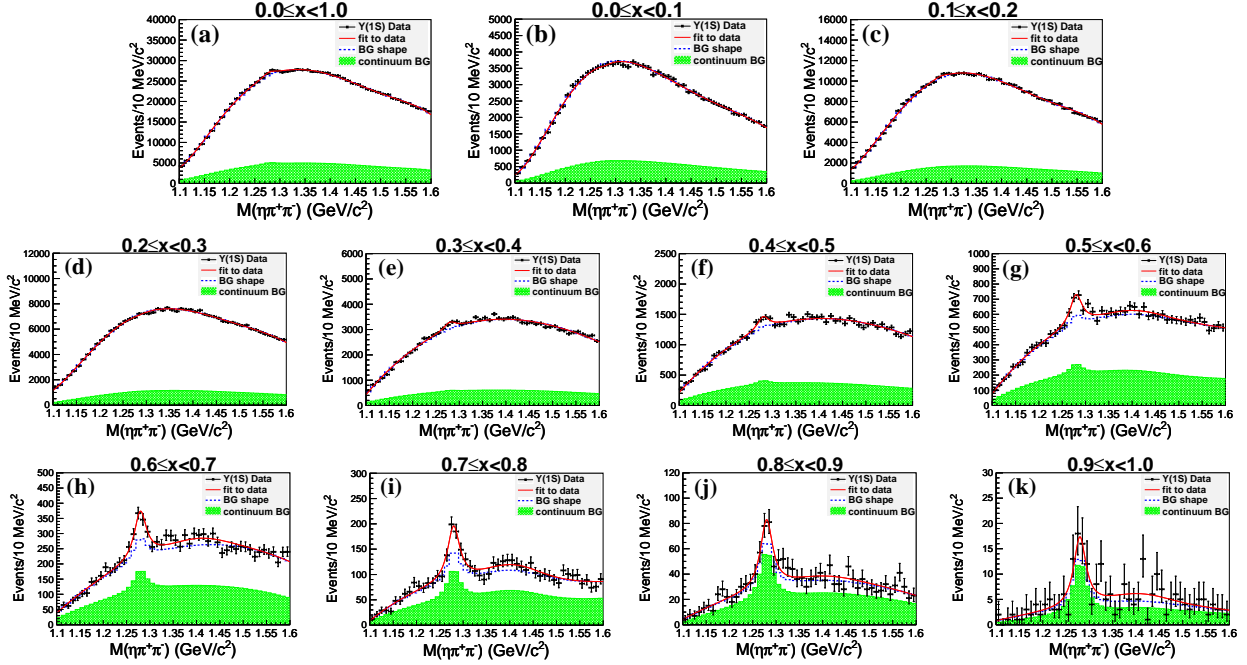


FIG. 2: (Color online) Invariant mass distributions of the $f_1(1285)$ candidates in (a) the entire x region and (b-k) for x bins of size 0.1. The dots with error bars are the $\Upsilon(1S)$ data. The red solid lines are the best fits, and the blue dotted lines represent the total backgrounds. The cross-hatched green histograms are from the normalized continuum contributions.

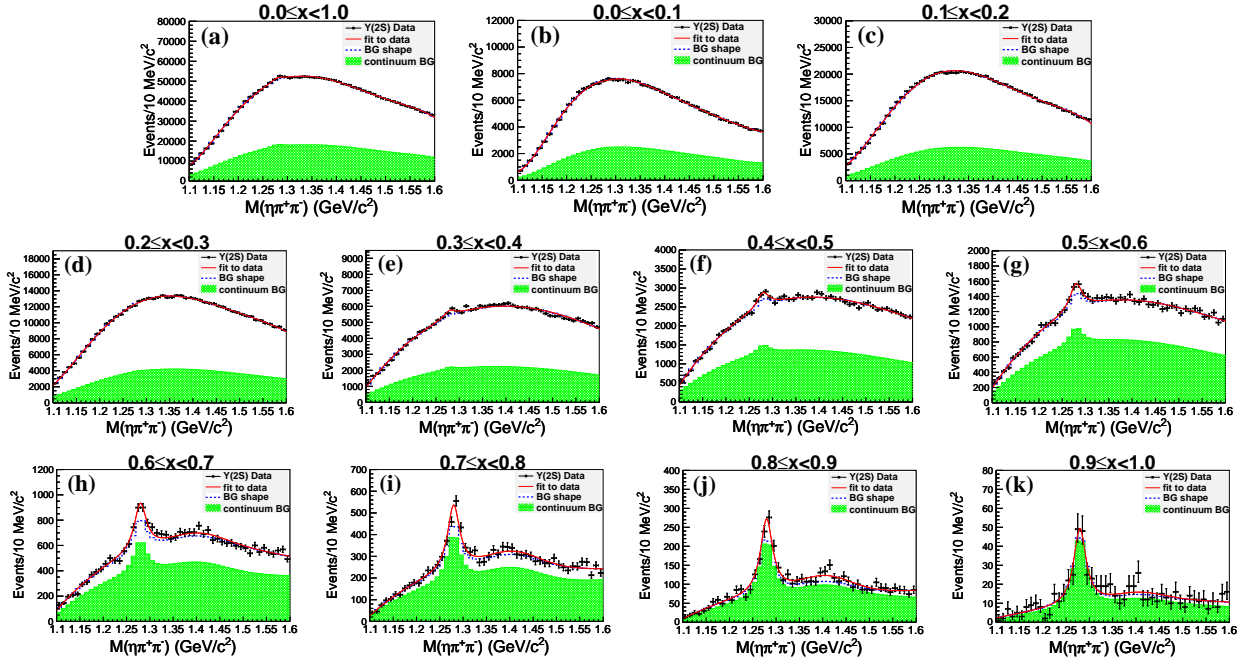


FIG. 3: (Color online) Invariant mass distributions of the $f_1(1285)$ candidates in (a) the entire x region and (b-k) for x bins of size 0.1. The dots with error bars are the $\Upsilon(2S)$ data. The red solid lines are the best fits, and the blue dotted lines represent the total backgrounds. The green cross-hatched histograms are from the normalized continuum contributions.

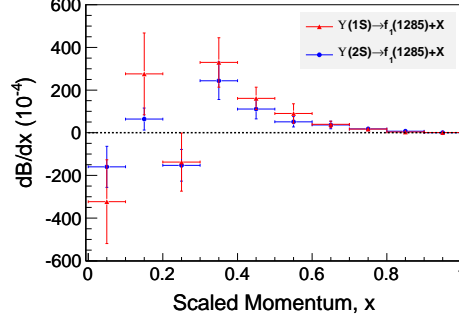


FIG. 4: (Color online) Differential branching fractions for $\Upsilon(1S)$ and $\Upsilon(2S)$ inclusive decays into $f_1(1285)$ as a function of the scaled momentum x defined in the text. The error bar of each point is the sum of the statistical and systematic errors.

IV. MEASUREMENTS OF $\chi_{bJ} \rightarrow J/\psi + \text{anything}$

The χ_{bJ} is identified through the decay $\Upsilon(2S) \rightarrow \gamma\chi_{bJ}$. The same mass regions of the J/ψ signal and sidebands are used as in Ref. [17], *i.e.*, we define the J/ψ signal region to be the window $|M_{\ell^+\ell^-} - m_{J/\psi}| < 0.03 \text{ GeV}/c^2$ ($\sim 2.5\sigma$), where $m_{J/\psi}$ is the J/ψ nominal mass [13], while the J/ψ sideband is $2.97 \text{ GeV}/c^2 < M_{\ell^+\ell^-} < 3.03 \text{ GeV}/c^2$ or $3.17 \text{ GeV}/c^2 < M_{\ell^+\ell^-} < 3.23 \text{ GeV}/c^2$, which is twice as wide as the signal region. After requiring the lepton-pair mass to be within the J/ψ signal region, Figs. 5 (a–c) show the distributions of the $\Upsilon(2S)$ radiative photon energy in the e^+e^- C.M. frame from MC simulated $\Upsilon(2S) \rightarrow \gamma\chi_{bJ}$, $\chi_{bJ} \rightarrow J/\psi + \text{anything}$ decays, where each χ_{bJ} signal shape is described by the convolution of a BW function with a Novosibirsk [29] function. Based on the fitted results, the efficiencies are $(23.87 \pm 0.42)\%$, $(32.21 \pm 0.53)\%$, and $(22.96 \pm 0.39)\%$ for χ_{b0} , χ_{b1} and χ_{b2} , respectively.

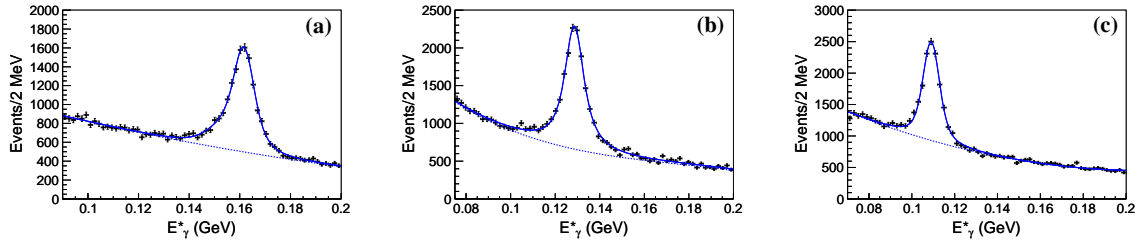


FIG. 5: The spectra of the $\Upsilon(2S)$ radiative photon energy in the e^+e^- C.M. frame from MC simulated $\Upsilon(2S) \rightarrow \gamma\chi_{bJ}$, $\chi_{bJ} \rightarrow J/\psi + \text{anything}$ signal samples for (a) χ_{b0} , (b) χ_{b1} and (c) χ_{b2} , respectively.

As shown in Fig. 6 of the spectrum of the $\Upsilon(2S)$ radiative photon energy in the C.M. frame, a clear χ_{b2} signal may be observed. After all selection requirements, no backgrounds showing peak distributions are found in the distribution estimated from J/ψ mass sideband data, nor in the continuum production in the χ_{bJ} signal regions, in agreement with the expectation from the $\Upsilon(2S)$ generic MC samples. An unbinned extended maximum-likelihood fit to the spectrum is performed to extract the signal and background yields in the $\Upsilon(2S)$ data samples. In the fit, the probability density function (PDF) of each χ_{bJ} signal is a BW function convolved with a Novosibirsk function with all the parameters free; for the background PDF, a third-order Chebyshev polynomial function is adopted. The fit yields 243 ± 101 , 269 ± 120 , and 462 ± 105 events for the χ_{b0} , χ_{b1} , and χ_{b2} signals, respectively, in the $\Upsilon(2S)$ data sample. The statistical significances of the χ_{b0} , χ_{b1} and χ_{b2} signals are estimated to be 1.5σ , 1.1σ and 3.5σ , from the differences of the logarithmic

likelihoods, $-2 \ln(\mathcal{L}_0/\mathcal{L}_{\max})$, where \mathcal{L}_0 and \mathcal{L}_{\max} are the likelihoods of the fits without and with a signal component, respectively (taking the number of degrees of freedom in each fit into account). For $\chi_{b2} \rightarrow J/\psi + \text{anything}$, the branching fraction is measured for the first time using

$$\mathcal{B}(\chi_{b2} \rightarrow J/\psi + \text{anything}) = \frac{N_{\chi_{b2}}}{N_{\Upsilon(2S)} \times \varepsilon_{\chi_{b2}} \times \mathcal{B}(\Upsilon(2S) \rightarrow \gamma\chi_{b2}) \times \mathcal{B}(J/\psi \rightarrow \ell^+\ell^-)},$$

where $N_{\chi_{b2}}$ is the number of fitted χ_{b2} signal events and $\varepsilon_{\chi_{b2}}$ is the signal detection efficiency given above. We measure a value of $(1.50 \pm 0.34(\text{stat.}) \pm 0.22(\text{syst.})) \times 10^{-3}$. The systematic uncertainties are discussed below. The $\chi_{b0,b1}$ branching fractions are computed in a similar way. Since the $\chi_{b0,b1}$ signal significances are less than 3σ , we compute 90% credibility level (C.L.) upper limits x^{UL} on the $\chi_{b0,b1}$ signal yields and the branching fractions. For this purpose, we solve the equation $\int_0^{x^{\text{UL}}} \mathcal{L}(x)dx / \int_0^{+\infty} \mathcal{L}(x)dx = 0.9$, where x is the assumed signal yield or branching fraction, and $\mathcal{L}(x)$ is the corresponding likelihood of the data. To take into account the systematic uncertainties discussed below, the likelihood is convolved with a Gaussian function whose width equals the total systematic uncertainty. The upper limits for the yields of χ_{b0} and χ_{b1} are 380 and 432 respectively, and the corresponding upper limits on the branching fractions are $\mathcal{B}^{\text{UL}}(\chi_{b0} \rightarrow J/\psi + \text{anything}) = 2.3 \times 10^{-3}$ and $\mathcal{B}^{\text{UL}}(\chi_{b1} \rightarrow J/\psi + \text{anything}) = 1.1 \times 10^{-3}$ at 90% C.L.

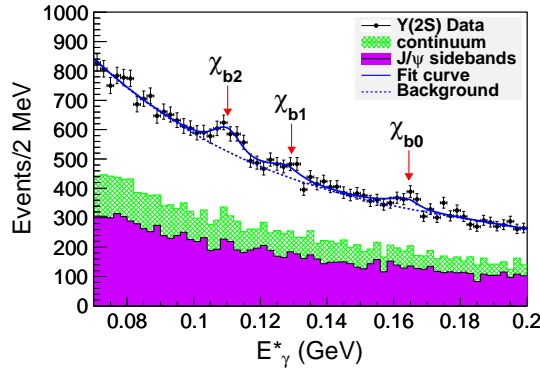


FIG. 6: (Color online) The spectra of the $\Upsilon(2S)$ radiative photon energy in the e^+e^- C.M. frame in $\Upsilon(2S)$ data. The dots with error bars are the $\Upsilon(2S)$ data. The blue solid line is the best fit, and the blue dotted line represents the backgrounds. The magenta shaded histogram is from the normalized J/ψ sideband and the green cross-hatched histogram is from the normalized continuum contributions described in the text.

V. MEASUREMENTS OF $\chi_{b1} \rightarrow \omega + \text{anything}$

Candidate ω mesons are reconstructed via $\pi^+\pi^-\pi^0$. We perform a mass-constrained kinematic fit to the selected π^0 candidate and require $\chi^2 < 10$. To remove the backgrounds with K_S^0 , the $\pi^+\pi^-$ invariant mass is required to be outside the $[0.475, 0.515]$ GeV/c^2 range. After requiring the $\pi^+\pi^-\pi^0$ invariant mass to be within the ω signal region of $0.755 \text{ GeV}/c^2 < M(\pi^+\pi^-\pi^0) < 0.805 \text{ GeV}/c^2$, Fig. 7 shows the distributions of the energy of the $\Upsilon(2S)$ radiative photon in the C.M. frame, where the dots represent the $\Upsilon(2S)$ data and the cross-hatched histogram is from the normalized continuum contributions. We define the χ_{b1} signal region as $0.12 \text{ GeV} < E_\gamma^* < 0.14 \text{ GeV}$ and its sideband as $0.075 \text{ GeV} < E_\gamma^* < 0.095 \text{ GeV}$ or $0.18 \text{ GeV} < E_\gamma^* < 0.20 \text{ GeV}$,

which is twice as wide as the signal region. From the histogram, no χ_{b1} signal is present in the continuum contributions.

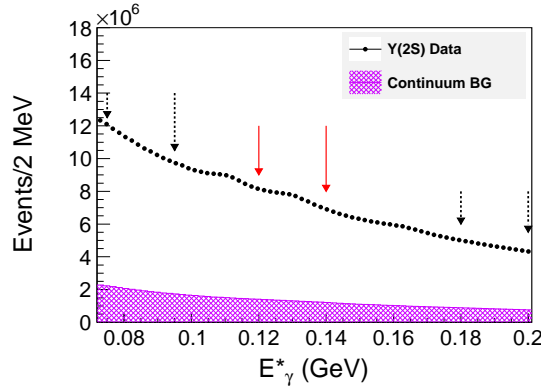


FIG. 7: (Color online) The spectra of the $\Upsilon(2S)$ radiative photon energy in the e^+e^- C.M. frame, where the dots with imperceptible error bars are the $\Upsilon(2S)$ data and the magenta cross-hatched histogram is from the normalized continuum contributions. The red solid arrows indicate the selected χ_{b1} signal region, and the black dashed arrows show the two ranges of the χ_{b1} sideband.

After the application of the above requirements, the $\pi^+\pi^-\pi^0$ invariant mass distribution from MC simulated $\chi_{b1} \rightarrow \omega + \text{anything}$ signal sample is shown in Fig. 8a. In the fit to this distribution, a Voigtian function is used for the ω signal shape and a second-order Chebyshev polynomial function is used for the background shape. Based on the fitted result, the efficiency is $(10.9 \pm 0.1)\%$. Figure 8b shows the distributions of the $\pi^+\pi^-\pi^0$ invariant mass from the $\Upsilon(2S)$ data (the dots with error bars) and the normalized χ_{b1} sideband events (the cross-hatched histogram). From the plot, the observed ω signals in the normalized χ_{b1} sideband account for most of the events in the χ_{b1} signal region.

A simultaneous binned extended maximum likelihood fit is applied to the $\pi^+\pi^-\pi^0$ invariant mass spectra to extract the ω signal yields in the χ_{b1} signal region and its sideband. The ω signal shape is described by a Voigtian function with the values of the parameters fixed to those from the fit to MC-simulated signals; a second-order Chebyshev polynomial background shape is used for the χ_{b1} decay backgrounds in addition to the normalized χ_{b1} sideband. The fitted ω signal yield is 51054 ± 12943 and the estimated statistical significance is 4.1σ . Hence, the branching fraction for $\chi_{b1} \rightarrow \omega + \text{anything}$ is measured for the first time to be

$$\mathcal{B}(\chi_{b1} \rightarrow \omega + \text{anything}) = (4.9 \pm 1.3(\text{stat.}) \pm 0.6(\text{syst.})) \times 10^{-2}.$$

VI. SEARCH FOR X_{tetra} IN $\Upsilon(1S)$, $\Upsilon(2S)$, AND χ_{b1} DECAYS

We generate a large number of MC samples for $\Upsilon(1S, 2S) \rightarrow \chi_{c1} + X_{\text{tetra}}$, $\Upsilon(1S, 2S) \rightarrow f_1(1285) + X_{\text{tetra}}$, $\chi_{b1} \rightarrow J/\psi + X_{\text{tetra}}$, and $\chi_{b1} \rightarrow \omega + X_{\text{tetra}}$ with X_{tetra} masses varying from 1.16 to 2.46 GeV/c^2 in steps of 0.10 GeV/c^2 and widths varying from 0.0 to 0.3 GeV in steps of 0.1 GeV , using the same decay modes as in Ref. [17]. After applying all the event selections in Ref. [17], all relevant efficiencies are obtained; they are displayed graphically in Fig. 9. Since the event selection requirements are independent of the recoil part of the χ_{c1} , $f_1(1285)$, J/ψ ,

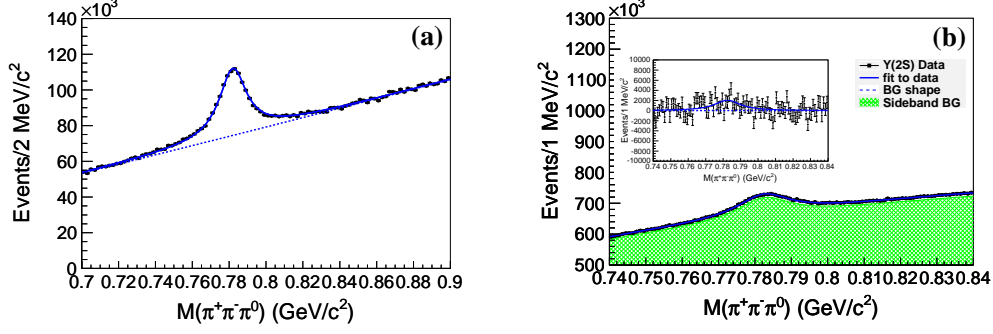


FIG. 8: (Color online) The $\pi^+\pi^-\pi^0$ invariant mass spectra from (a) MC simulated $\chi_{b1} \rightarrow \omega + \text{anything}$ signal sample and (b) $\Upsilon(2S)$ data. The dots represent the data. The cross-hatched histogram in (b) represents the normalized χ_{b1} sideband; the inset shows the fitted background-subtracted distribution. The blue solid lines are the best fits, and the blue dotted lines represent the backgrounds.

and ω in the studied channels, the detection efficiencies are only related to the recoil masses. The efficiencies versus X_{tetra} mass in the entire region from 1.16 to 3.0 GeV/c^2 are displayed graphically in Fig. 9 for the studied production modes. The fitted curves show the second-order Chebyshev polynomials used to model these efficiencies.

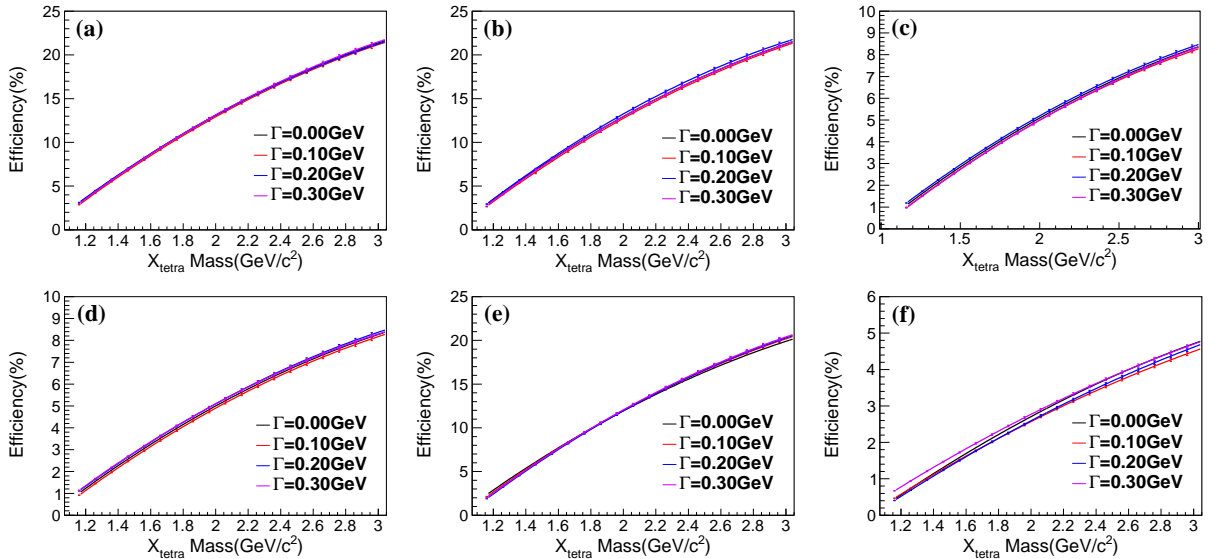


FIG. 9: (Color online) Reconstruction efficiencies for (a) $\Upsilon(1S) \rightarrow \chi_{c1} + X_{\text{tetra}}$, (b) $\Upsilon(2S) \rightarrow \chi_{c1} + X_{\text{tetra}}$, (c) $\Upsilon(1S) \rightarrow f_1(1285) + X_{\text{tetra}}$, (d) $\Upsilon(2S) \rightarrow f_1(1285) + X_{\text{tetra}}$, (e) $\chi_{b1} \rightarrow J/\psi + X_{\text{tetra}}$ and (f) $\chi_{b1} \rightarrow \omega + X_{\text{tetra}}$ as a function of the assumed X_{tetra} masses, with X_{tetra} widths varying from 0.0 to 0.3 GeV in steps of 0.1 GeV. The four solid lines in each panel, one for each X_{tetra} width, are the fits of a second-order Chebyshev polynomial to these data.

In the channels analyzed below, $\Upsilon(1S, 2S) \rightarrow \chi_{c1} + X_{\text{tetra}}$, $\Upsilon(1S, 2S) \rightarrow f_1(1285) + X_{\text{tetra}}$, $\chi_{b1} \rightarrow J/\psi + X_{\text{tetra}}$, and $\chi_{b1} \rightarrow \omega + X_{\text{tetra}}$, we search for the X_{tetra} signals in the recoil mass spectra of the χ_{c1} , $f_1(1285)$, J/ψ , and ω , respectively, with X_{tetra} widths between 0.0 and 0.3 GeV in steps of 0.1 GeV. All recoil mass spectra are taken from Ref. [17] with a focused view of the low-mass region.

For $\Upsilon(1S, 2S) \rightarrow \chi_{c1} + X_{\text{tetra}}$, the χ_{c1} is reconstructed via its decay into $\gamma J/\psi$, $J/\psi \rightarrow \ell^+\ell^-$

($\ell = e$ or μ). Figure 10 shows the recoil mass spectra of χ_{c1} candidates in the $\Upsilon(1S, 2S)$ data, where the shaded histograms are from the normalized χ_{c1} sideband and the cross-hatched histograms show the normalized continuum contributions. See Ref. [17] for the definition of the χ_{c1} sideband and the normalization method of the continuum contribution. There are no evident signals for any of the X_{tetra} states at any of the masses. In the entire region of study, the most significant signal is observed at an X_{tetra} mass of 2.46 (2.26) GeV/c^2 and width of 0.3 (0.0) GeV with a statistical significance of 1.4σ (0.6σ) in $\Upsilon(1S)$ ($\Upsilon(2S)$) data. Since the number of selected signal candidate events is small, we obtain the 90% C.L. upper limit of the signal yield (N^{UL}) at each X_{tetra} mass point by using the frequentist approach [30] implemented in the POLE (Poissonian limit estimator) program [31], where each mass region is selected to contain 95% of the signal according to MC simulations, the number of observed signal events is counted directly, and the number of expected background events is estimated from the sum of the normalized χ_{c1} sideband and continuum contributions. The systematic uncertainties discussed below are taken into account.

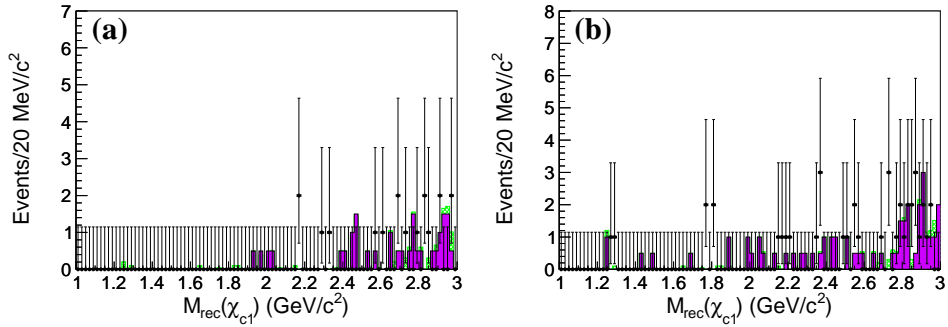


FIG. 10: (Color online) The χ_{c1} recoil mass spectra in the (a) $\Upsilon(1S)$ and (b) $\Upsilon(2S)$ data samples. The shaded histograms are from the normalized χ_{c1} sideband and the cross-hatched histograms show the normalized continuum contributions [17].

The calculated upper limits on the numbers of signal events (N^{UL}) and branching fraction (\mathcal{B}^{UL}) for each X_{tetra} state with X_{tetra} masses from 1.16 to 2.46 GeV/c^2 and widths from 0.0 to 0.3 GeV in $\Upsilon(1S, 2S)$ data are listed in Table II, together with the reconstruction efficiencies (ϵ) and the systematic uncertainties (σ_{sys}). The results are displayed graphically in Fig. 11.

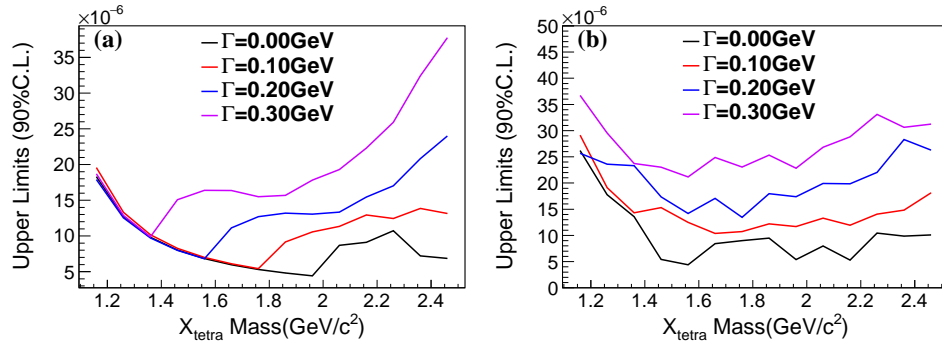


FIG. 11: (Color online) The upper limits on the branching fractions for (a) $\Upsilon(1S) \rightarrow \chi_{c1} + X_{\text{tetra}}$ and (b) $\Upsilon(2S) \rightarrow \chi_{c1} + X_{\text{tetra}}$ as a function of the assumed X_{tetra} mass with widths fixed at 0.0, 0.1, 0.2, and 0.3 GeV .

For $\Upsilon(1S, 2S) \rightarrow f_1(1285) + X_{\text{tetra}}$, $f_1(1285)$ candidates are reconstructed via $\eta\pi^+\pi^-$, $\eta \rightarrow$

$\gamma\gamma$. Figure 12 shows the recoil mass spectra of the $f_1(1285)$ in $\Upsilon(1S, 2S)$ data, together with the backgrounds from the normalized $f_1(1285)$ sideband and the normalized continuum contributions. No evident X_{tetra} signals are seen. An unbinned extended maximum-likelihood fit repeated with X_{tetra} masses from 1.46 to 2.46 GeV/c^2 in steps of 0.10 GeV/c^2 , and with X_{tetra} widths from 0.0 to 0.3 GeV in steps of 0.1 GeV , is applied to the recoil mass spectra. The signal shape of each X_{tetra} signal is described with a BW function convolved with a Novosibirsk function, where all parameter values are fixed to those from the fit to the MC-simulated signals. Since no backgrounds showing peak distributions are found, a second-order Chebyshev polynomial shape is used for the backgrounds. The fit result for the X_{tetra} signal with its mass fixed at 1.66 GeV/c^2 (a theoretically predicted mass for a scalar tetraquark state [16]) and width fixed at 0.10 GeV is shown in Fig. 12. The fit yields 1.7 ± 4.7 (-0.3 ± 9.8) events for the X_{tetra} signals in the $\Upsilon(1S)$ ($\Upsilon(2S)$) data sample. In the whole mass region of interest, the most significant signal is observed at an X_{tetra} mass of 2.26 (2.16) GeV/c^2 and width of 0.0 (0.3) GeV with a statistical significance of 1.1σ (1.8σ) in $\Upsilon(1S)$ ($\Upsilon(2S)$) data.

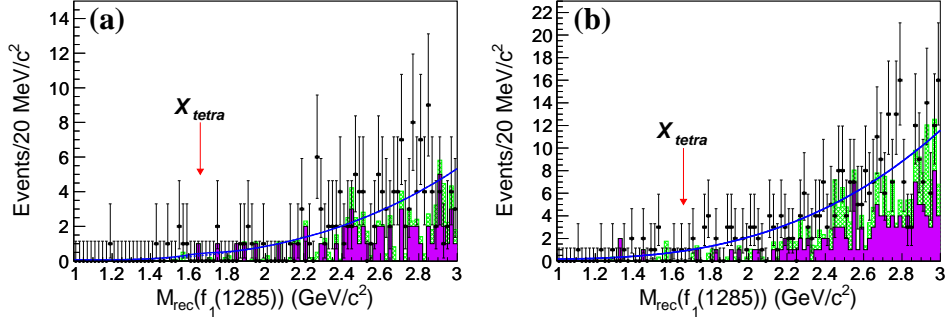


FIG. 12: (Color online) The $f_1(1285)$ recoil mass spectra in the (a) $\Upsilon(1S)$ and (b) $\Upsilon(2S)$ data samples. The blue solid curves show the results of the fit described in the text, including the X_{tetra} states with widths fixed at 0.10 GeV and masses fixed at 1.66 GeV/c^2 indicated by the arrows. The nearly imperceptible blue dashed curves show the fitted background. The magenta shaded histograms are from the normalized $f_1(1285)$ sideband and the green cross-hatched histograms show the normalized continuum contributions.

For $\chi_{b1} \rightarrow J/\psi + X_{\text{tetra}}$, the χ_{b1} is identified through the decay $\Upsilon(2S) \rightarrow \gamma\chi_{b1}$. Figure 13 shows the recoil mass spectrum of $\gamma J/\psi$ in $\Upsilon(2S)$ data, together with the background estimated from the normalized J/ψ sideband and the normalized continuum contributions. No evident X_{tetra} signal is observed. An unbinned extended maximum-likelihood fit is applied to the $\gamma J/\psi$ recoil mass spectrum. The result of the fit with the X_{tetra} mass fixed at 1.66 GeV/c^2 and width fixed at 0.10 GeV is shown in Fig. 13. This fit yields 8.9 ± 5.8 X_{tetra} signal events. In the entire region of study, the most significant signal is observed at an X_{tetra} mass of 1.76 GeV/c^2 and width of 0.1 GeV , with a statistical significance of 2.8σ .

For $\chi_{b1} \rightarrow \omega + X_{\text{tetra}}$, ω candidates are reconstructed via $\pi^+\pi^-\pi^0$, $\pi^0 \rightarrow \gamma\gamma$. Figure 14 shows the recoil mass spectrum of $\gamma\omega$ for events in the ω signal region, along with the backgrounds from the normalized ω sideband and the normalized continuum contributions. No evident X_{tetra} signal is observed. An unbinned extended maximum-likelihood fit is applied to the $\gamma\omega$ recoil mass spectrum. The result of the fit including the X_{tetra} signal with its mass fixed at 1.66 GeV/c^2 and width fixed at 0.10 GeV is shown in Fig. 14. This fit yields -7.8 ± 9.1 X_{tetra} signal events. In the entire region of study, the most significant signal is observed at an X_{tetra} mass of 2.26 GeV/c^2 and width of 0.1 GeV , with a statistical significance of 2.2σ .

Considering the yields for $\Upsilon(1S, 2S) \rightarrow f_1(1285) + X_{\text{tetra}}$, $\chi_{b1} \rightarrow J/\psi + X_{\text{tetra}}$ and $\chi_{b1} \rightarrow$

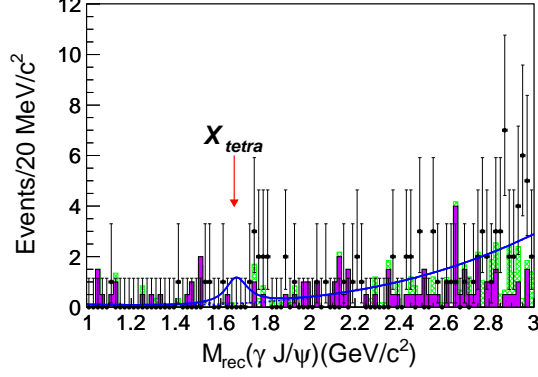


FIG. 13: (Color online) The $\gamma J/\psi$ recoil mass spectrum for $\Upsilon(2S) \rightarrow \gamma\chi_{b1} \rightarrow \gamma J/\psi + \text{anything}$ in the $\Upsilon(2S)$ data sample. The blue solid curve shows the result of the fit described in the text, including the X_{tetra} state with a width fixed to 0.10 GeV and a mass fixed at 1.66 GeV/c^2 indicated by the arrow. The blue dashed curve shows the fitted background. The magenta shaded histogram is from the normalized J/ψ sideband and the green cross-hatched histogram shows the normalized continuum contributions.

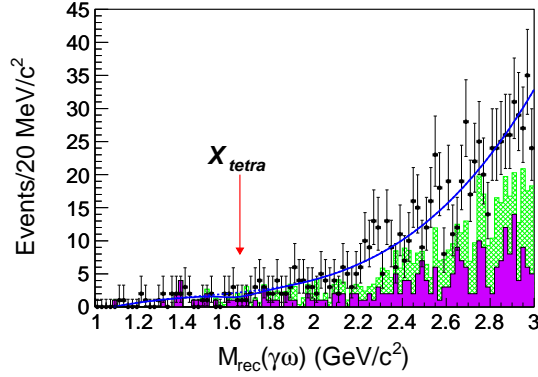


FIG. 14: (Color online) The $\gamma\omega$ recoil mass spectrum for $\Upsilon(2S) \rightarrow \gamma\chi_{b1} \rightarrow \gamma\omega + \text{anything}$ in the $\Upsilon(2S)$ data sample. The blue solid curve shows the result of the fit described in the text, including the X_{tetra} state with a width fixed to 0.10 GeV and a mass fixed at 1.66 GeV/c^2 indicated by the arrow. The blue dashed curve shows the fitted background. The magenta shaded histogram is from the normalized ω sideband and the green cross-hatched histogram shows the normalized continuum contributions.

$\omega + X_{\text{tetra}}$ are very small, we determine the 90% C.L. upper limits on the X_{tetra} signal yields (N^{UL}) for $M(X_{\text{tetra}}) < 1.46 \text{ GeV}/c^2$ following the procedure in Ref. [31] as described above for $\Upsilon(1S, 2S) \rightarrow \chi_{c1} + X_{\text{tetra}}$, and for $M(X_{\text{tetra}}) > 1.46 \text{ GeV}/c^2$ using the same method as described for $\chi_{b0,b1} \rightarrow J/\psi + \text{anything}$. Here, the systematic errors have been taken into account in the determination of N^{UL} .

The calculated upper limits on the numbers of signal events (N^{UL}) and branching fraction (\mathcal{B}^{UL}) for $\Upsilon(1S, 2S) \rightarrow f_1(1285) + X_{\text{tetra}}$, $\chi_{b1} \rightarrow J/\psi + X_{\text{tetra}}$ and $\chi_{b1} \rightarrow \omega + X_{\text{tetra}}$ with X_{tetra} masses from 1.16 to 2.46 GeV/c^2 and widths from 0.0 to 0.3 GeV are listed in Table II, together with the reconstruction efficiencies (ε) and the systematic uncertainties (σ_{sys}). The results are displayed graphically in Fig. 15.

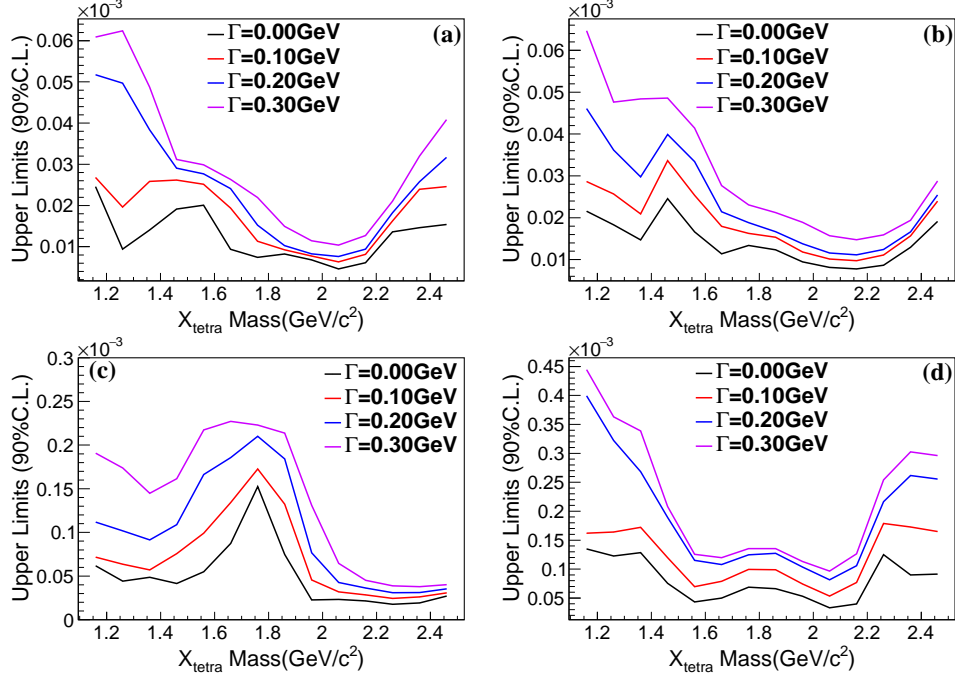


FIG. 15: (Color online) The upper limits on the branching fractions for (a) $\Upsilon(1S) \rightarrow f_1(1285) + X_{\text{tetra}}$, (b) $\Upsilon(2S) \rightarrow f_1(1285) + X_{\text{tetra}}$, (c) $\chi_{b1} \rightarrow J/\psi + X_{\text{tetra}}$, and (d) $\chi_{b1} \rightarrow \omega + X_{\text{tetra}}$ as a function of the assumed X_{tetra} mass with widths fixed at 0.0, 0.1, 0.2, and 0.3 GeV, respectively.

VII. SYSTEMATIC UNCERTAINTIES

Most of the systematic errors in the branching fraction measurements are the same as in Ref. [17], including tracking reconstruction, photon reconstruction, particle identification, trigger efficiency, the branching fractions of the intermediate states, and the total numbers of $\Upsilon(1S)$ and $\Upsilon(2S)$ events; the notable exception is the dominant systematic error from the fit uncertainty. By changing the order of the background polynomial and the range of the fit, the model-dependent relative difference in the signal yields (or the upper limits for those modes with statistically insignificant branching fractions) is obtained; this is taken as the systematic error due to the uncertainty of the fit. The estimation of the continuum contributions in the $f_1(1285)$ inclusive production processes assumes a $1/s^2$ dependence. The analysis is repeated assuming a $1/s$ or $1/s^3$ dependence and the largest change in the fitted $f_1(1285)$ signal yield is taken as a systematic uncertainty. Assuming that all of these systematic-error sources are independent, the total systematic errors are summed in quadrature and listed in Table II for all the studied modes for each hypothesized X_{tetra} mass.

VIII. SUMMARY

In summary, utilizing the recoil mass spectra of the χ_{c1} , $f_1(1285)$, J/ψ , and ω in the channels $\Upsilon(1S, 2S) \rightarrow \chi_{c1} + G_{0--}$, $\Upsilon(1S, 2S) \rightarrow f_1(1285) + G_{0--}$, $\chi_{b1} \rightarrow J/\psi + G_{0--}$, and $\chi_{b1} \rightarrow \omega + G_{0--}$ [17], respectively, we report the first search for the light tetraquark states predicted with a mass of $1.66 \pm 0.14 \text{ GeV}/c^2$ and $J^{PC} = 0^{--}$, and with a mass in the region 1.18–1.43 GeV/c^2 and $J^{PC} = 1^{+-}$ [16]. No evident signal is found below 3 GeV/c^2 in the above processes

and 90% C.L. upper limits are set on the branching fractions. Figures 11 and 15 show the upper limits on the branching fractions as a function of the tetraquark masses. In addition, as byproducts of the search, we measure the inclusive $f_1(1285)$ production in $\Upsilon(1S, 2S)$, J/ψ production in $\chi_{bJ}(J = 0, 1, 2)$, and ω production in χ_{b1} . The corresponding branching fractions are measured for the first time to be $\mathcal{B}(\Upsilon(1S) \rightarrow f_1(1285) + \text{anything}) = (46 \pm 28(\text{stat.}) \pm 13(\text{syst.})) \times 10^{-4}$, $\mathcal{B}(\Upsilon(2S) \rightarrow f_1(1285) + \text{anything}) = (22 \pm 15(\text{stat.}) \pm 6.3(\text{syst.})) \times 10^{-4}$, $\mathcal{B}(\chi_{b2} \rightarrow J/\psi + \text{anything}) = (1.50 \pm 0.34(\text{stat.}) \pm 0.22(\text{syst.})) \times 10^{-3}$, and $\mathcal{B}(\chi_{b1} \rightarrow \omega + \text{anything}) = (4.9 \pm 1.3(\text{stat.}) \pm 0.6(\text{syst.})) \times 10^{-2}$, and the 90% C.L. upper limits on the branching fractions $\mathcal{B}(\chi_{b0} \rightarrow J/\psi + \text{anything}) < 2.3 \times 10^{-3}$ and $\mathcal{B}(\chi_{b1} \rightarrow J/\psi + \text{anything}) < 1.1 \times 10^{-3}$ are determined for the first time.

IX. ACKNOWLEDGMENTS

We thank the KEKB group for the excellent operation of the accelerator; the KEK cryogenics group for the efficient operation of the solenoid; and the KEK computer group, the National Institute of Informatics, and the PNNL/EMSL computing group for valuable computing and SINET5 network support. We acknowledge support from the Ministry of Education, Culture, Sports, Science, and Technology (MEXT) of Japan, the Japan Society for the Promotion of Science (JSPS), and the Tau-Lepton Physics Research Center of Nagoya University; the Australian Research Council; Austrian Science Fund under Grant No. P 26794-N20; the National Natural Science Foundation of China under Contracts No. 10575109, No. 10775142, No. 10875115, No. 11175187, No. 11475187, No. 11521505 and No. 11575017; the Chinese Academy of Science Center for Excellence in Particle Physics; the Ministry of Education, Youth and Sports of the Czech Republic under Contract No. LTT17020; the Carl Zeiss Foundation, the Deutsche Forschungsgemeinschaft, the Excellence Cluster Universe, and the VolkswagenStiftung; the Department of Science and Technology of India; the Istituto Nazionale di Fisica Nucleare of Italy; the WCU program of the Ministry of Education, National Research Foundation (NRF) of Korea Grants No. 2011-0029457, No. 2012-0008143, No. 2014R1A2A2A01005286, No. 2014R1A2A2A01002734, No. 2015R1A2A2A01003280, No. 2015H1A2A1033649, No. 2016R1D1A1B01010135, No. 2016K1A3A7A09005603, No. 2016K1A3A7A09005604, No. 2016R1D1A1B02012900, No. 2016K1A3A7A09005606, No. NRF-2013K1A3A7A06056592; the Brain Korea 21-Plus program, Radiation Science Research Institute, Foreign Large-size Research Facility Application Supporting project and the Global Science Experimental Data Hub Center of the Korea Institute of Science and Technology Information; the Polish Ministry of Science and Higher Education and the National Science Center; the Ministry of Education and Science of the Russian Federation and the Russian Foundation for Basic Research; the Slovenian Research Agency; Ikerbasque, Basque Foundation for Science and MINECO (Juan de la Cierva), Spain; the Swiss National Science Foundation; the Ministry of Education and the Ministry of Science and Technology of Taiwan; and the U.S. Department of Energy and the National Science Foundation.

-
- [1] N. Brambilla, S. Eidelman, P. Foka, S. Gardner, A. Kronfeld *et al.*, Eur. Phys. J. C **74**, 2981 (2014).
[2] A. Esposito, A. L. Guerrieri, F. Piccinini, A. Pilloni and A. D. Polosa, Int. J. Mod. Phys. A **30**, 1530002 (2015).

TABLE II: Summary of the upper limits for $\Upsilon(1S, 2S) \rightarrow \chi_{c1} + X_{\text{tetra}}$, $f_1(1285) + X_{\text{tetra}}$, and $\chi_{b1} \rightarrow J/\psi + X_{\text{tetra}}$, $\omega + X_{\text{tetra}}$ under different assumptions of X_{tetra} mass (m in GeV/c^2) and width (Γ in GeV), where N^{UL} is the upper limit on the number of signal events taking into account systematic errors, ε is the reconstruction efficiency, σ_{syst} is the total relative systematic uncertainty on the branching fraction and \mathcal{B}^{UL} is the 90% C.L. upper limit on the branching fraction.

m	$\Upsilon(1S) \rightarrow \chi_{c1} + X_{\text{tetra}}$ (for $\Gamma = 0.0/0.1/0.2/0.3$ GeV)				$\Upsilon(2S) \rightarrow \chi_{c1} + X_{\text{tetra}}$ (for $\Gamma = 0.0/0.1/0.2/0.3$ GeV)			
	$\varepsilon(\%)$	N^{UL}	$\sigma_{\text{syst}}(\%)$	$\mathcal{B}^{\text{UL}} (\times 10^{-6})$	$\varepsilon(\%)$	N^{UL}	$\sigma_{\text{syst}}(\%)$	$\mathcal{B}^{\text{UL}} (\times 10^{-6})$
1.16	3.1/2.9/3.1/3.0	2.3	6.2	18.3/19.6/17.9/18.7	3.0/2.6/3.0/2.7	4.7/4.7/4.7/6.0	6.3	26.2/29.1/25.7/36.7
1.26	4.4/4.2/4.5/4.3	2.3	6.2	12.7/13.3/12.5/12.9	4.3/4.0/4.2/4.1	4.7/4.7/6.0/7.6	6.3	17.8/19.1/23.6/29.5
1.36	5.7/5.5/5.8/5.7	2.3	6.2	9.8/10.1/9.7/9.9	5.7/5.4/5.6/5.5	4.7/4.7/7.9/7.9	6.3	13.6/14.3/23.3/23.7
1.46	7.0/6.8/7.0/7.0	2.3/2.3/2.3/4.2	6.2	8.0/8.3/8.0/15.1	6.7/6.5/7.0/6.9	2.3/5.9/7.6/10.0	6.3	5.4/15.3/17.4/23.0
1.56	8.2/8.0/8.2/8.2	2.3/2.3/2.3/5.5	6.2	6.8/7.0/6.8/16.4	8.2/8.0/8.1/8.1	2.3/5.9/7.0/10.5	6.3	4.4/12.5/14.2/21.2
1.66	9.4/9.2/9.4/9.4	2.3/2.3/4.2/6.1	6.2	6.0/6.1/11.1/16.4	9.2/9.0/9.3/9.3	4.7/5.8/10.0/14.4	6.3	8.4/10.4/17.1/24.9
1.76	10.5/10.3/10.5/10.5	2.3/2.3/5.5/6.5	6.2	5.3/5.4/12.7/15.5	10.3/10.1/10.4/10.3	5.8/6.7/8.8/14.9	6.3	9.0/10.7/13.5/23.0
1.86	11.6/11.4/11.6/11.6	2.3/4.2/6.1/7.1	6.2	4.8/9.2/13.2/15.7	11.4/11.2/11.3/11.4	6.7/8.7/12.1/17.8	6.3	9.5/12.2/18.0/25.3
1.96	12.7/12.7/12.5/12.7	2.3/5.5/6.5/9.2	6.2	4.4/10.6/13.0/17.8	12.5/12.5/12.4/12.5	4.2/9.3/13.5/17.3	6.3	5.4/11.6/17.4/22.8
2.06	13.7/13.5/13.7/13.7	4.1/6.1/7.1/10.2	6.2	8.7/11.3/13.3/19.3	13.6/13.4/13.5/13.5	6.7/11.2/16.7/21.1	6.3	8.0/13.3/19.9/26.8
2.16	14.7/14.5/14.6/14.7	5.5/7.2/9.2/12.9	6.2	9.1/12.9/15.4/22.3	14.6/14.4/14.5/14.5	4.7/10.5/17.3/24.6	6.3	5.3/11.9/19.8/28.8
2.26	15.6/15.4/15.6/15.7	6.5/7.3/10.2/16.4	6.2	10.7/12.4/17.0/25.9	15.5/15.3/15.5/15.4	10.1/13.5/20.7/30.4	6.3	10.4/14.1/22.0/33.1
2.36	16.6/16.4/16.5/16.6	4.1/9.3/13.8/20.7	6.2	7.2/13.8/20.8/32.4	16.4/16.2/16.4/16.4	10.1/14.3/29.3/30.0	6.3	9.9/14.8/28.3/30.6
2.46	17.4/17.2/17.4/17.5	4.1/9.3/16.9/24.3	6.2	6.8/13.2/24.0/37.8	17.3/17.1/17.3/17.3	10.4/18.7/27.7/32.3	6.3	10.1/18.1/26.3/31.2
m	$\Upsilon(1S) \rightarrow f_1(1285) + X_{\text{tetra}}$ (for $\Gamma = 0.0/0.1/0.2/0.3$ GeV)				$\Upsilon(2S) \rightarrow f_1(1285) + X_{\text{tetra}}$ (for $\Gamma = 0.0/0.1/0.2/0.3$ GeV)			
	$\varepsilon(\%)$	N^{UL}	$\sigma_{\text{syst}}(\%)$	$\mathcal{B}^{\text{UL}} (\times 10^{-6})$	$\varepsilon(\%)$	N^{UL}	$\sigma_{\text{syst}}(\%)$	$\mathcal{B}^{\text{UL}} (\times 10^{-6})$
1.16	1.2/1.1/1.0/1.0	4.4/4.4/7.8/9.1	20.2	24.5/26.8/51.7/60.9	1.0/0.9/1.0/1.0	5.1/6.0/10.8/15.1	20.2	21.6/28.6/46.1/64.7
1.26	1.6/1.5/1.7/1.5	2.3/4.4/12.7/14.1	20.2	9.4/19.6/49.7/62.4	1.5/1.4/1.6/1.5	6.4/8.4/13.5/16.6	20.2	18.3/25.7/36.2/47.6
1.36	2.1/2.0/2.2/2.0	4.4/7.8/12.7/14.8	20.2	14.0/25.9/38.4/48.8	2.1/2.0/2.2/2.0	7.2/9.8/15.3/22.7	20.2	14.7/20.9/29.8/48.4
1.46	2.6/2.7/2.5/2.5	7.6/10.7/11.0/11.6	20.9/21.6/22.2/24.4	19.1/26.2/29.1/31.2	2.6/2.5/2.5/2.4	15.0/19.7/23.3/27.3	20.4/24.9/27.8/28.6	24.5/33.6/39.9/48.6
1.56	3.2/3.2/3.1/3.0	9.7/12.1/12.9/13.4	20.2/20.2/21.5/22.2	20.0/25.2/27.7/29.9	3.0/3.0/3.1/3.0	12.1/17.9/24.2/28.9	20.1/20.4/22.3/24.4	16.6/25.4/33.4/41.4
1.66	3.6/3.5/3.7/3.5	5.2/10.3/13.4/13.9	20.5/21.7/22.0/24.5	9.4/19.4/24.1/26.3	3.5/3.4/3.6/3.5	9.3/14.3/18.1/22.5	22.0/23.2/23.5/28.3	11.4/17.9/21.4/27.7
1.76	4.1/4.0/4.2/4.0	4.5/6.8/9.8/13.3	20.5/21.6/24.2/24.3	7.4/11.3/15.2/21.9	4.0/3.9/4.1/4.0	12.5/14.9/18.2/21.4	20.8/23.6/24.5/29.1	13.4/16.3/18.8/23.1
1.86	4.5/4.4/4.6/4.4	5.5/6.6/7.1/9.9	20.3/20.5/21.0/22.3	8.2/9.2/10.2/14.9	4.4/4.3/4.5/4.4	12.7/15.4/17.4/21.7	20.5/21.4/21.5/23.0	12.8/15.3/16.7/21.2
1.96	4.9/4.8/5.0/4.8	5.1/5.8/6.2/8.3	20.3/20.3/20.6/21.0	6.8/7.7/8.2/11.4	4.8/4.7/4.9/4.7	10.6/12.9/15.9/20.8	20.2/20.6/27.0/23.7	9.4/11.8/13.8/18.9
2.06	5.3/5.2/5.4/5.2	3.7/5.0/6.2/8.1	20.0/20.2/20.2/20.3	4.6/6.3/7.6/10.4	5.2/5.1/5.3/5.1	9.9/12.0/14.3/18.8	24.8/26.0/27.0/27.5	8.1/10.1/11.6/15.7
2.16	5.7/5.6/5.8/5.6	5.3/6.9/8.2/10.8	20.4/21.7/23.7/24.2	6.1/8.2/9.4/12.7	5.6/5.5/5.7/5.5	10.2/12.6/14.8/19.0	26.7/27.4/30.8/33.6	7.8/9.7/11.1/14.7
2.26	6.1/6.0/6.2/6.0	12.6/14.7/17.0/19.0	21.4/24.0/24.2/30.9	13.6/16.2/18.2/21.0	6.0/5.9/6.1/5.9	12.1/15.3/17.8/22.0	21.5/24.8/28.8/35.2	8.6/11.1/12.4/15.9
2.36	6.5/6.4/6.6/6.4	14.2/22.8/25.7/30.7	24.5/27.7/28.8/32.9	14.6/23.9/25.8/32.0	6.4/6.3/6.5/6.4	19.4/23.0/25.3/28.6	20.6/25.6/26.5/28.0	12.9/15.7/16.6/19.4
2.46	6.8/6.7/6.9/6.7	15.9/24.8/32.4/40.1	20.6/21.1/21.2/22.3	15.4/24.6/31.7/40.8	6.7/6.6/6.8/6.6	29.7/36.8/40.1/42.7	20.9/22.2/23.5/29.9	19.1/23.9/25.4/28.7
m	$\chi_{b1} \rightarrow J/\psi + X_{\text{tetra}}$ (for $\Gamma = 0.0/0.1/0.2/0.3$ GeV)				$\chi_{b1} \rightarrow \omega + X_{\text{tetra}}$ (for $\Gamma = 0.0/0.1/0.2/0.3$ GeV)			
	$\varepsilon(\%)$	N^{UL}	$\sigma_{\text{syst}}(\%)$	$\mathcal{B}^{\text{UL}} (\times 10^{-5})$	$\varepsilon(\%)$	N^{UL}	$\sigma_{\text{syst}}(\%)$	$\mathcal{B}^{\text{UL}} (\times 10^{-5})$
1.16	2.4/2.5/2.3/2.3	1.9/2.3/3.3/5.6	7.8	6.2/7.2/11.1/8/19.1	0.4/0.5/0.4/0.6	5.7/7.2/15.3/24.0	9.3	13.5/16.2/40.0/44.4
1.26	3.7/3.8/3.6/3.6	2.1/3.1/4.6/8.0	7.8	4.4/6.4/10.2/17.4	0.7/0.7/0.7/0.7	8.6/11.6/21.1/25.6	9.3	12.2/16.4/32.2/26.3
1.36	4.9/5.0/4.8/4.9	3.1/3.7/5.6/9.0	7.8	4.9/5.7/9.1/14.5	1.0/1.0/1.0/1.1	12.6/16.5/24.6/34.4	9.3	12.8/17.2/26.8/33.9
1.46	6.1/6.2/6.0/6.1	3.3/6.0/8.4/12.5	7.9/8.7/10.1/13.9	4.2/7.6/10.9/16.2	1.3/1.3/1.2/1.4	9.4/14.5/22.3/27.1	19.0/20.3/21.4/23.5	7.5/12.0/18.9/20.8
1.56	7.3/7.4/7.2/7.3	5.2/9.4/15.3/20.2	7.9/8.1/8.3/9.1	5.5/9.9/16.7/21.7	1.6/1.5/1.5/1.6	6.6/10.1/16.4/19.3	11.4/14.0/18.6/19.8	4.3/7.0/11.4/12.6
1.66	8.4/8.5/8.3/8.4	9.4/14.6/19.8/24.4	7.9/8.0/11.4/12.4	8.7/13.4/18.6/22.7	1.9/1.8/1.8/1.9	8.8/13.2/18.0/21.2	13.1/13.9/16.4/16.9	5.0/7.9/10.8/12.0
1.76	9.5/9.6/9.4/9.5	18.6/21.3/25.4/27.1	8.1/9.0/9.9/12.0	15.2/17.2/21.0/22.3	2.1/2.0/2.0/2.1	13.9/19.0/23.8/27.1	9.5/10.9/13.4/13.7	6.9/9.9/12.4/13.5
1.86	10.6/10.7/10.5/10.6	10.2/18.2/24.8/28.7	7.9/8.6/8.9/10.4	7.5/13.2/18.4/21.4	2.4/2.2/2.2/2.4	15.0/21.3/27.3/30.2	10.0/11.0/11.1/11.3	6.6/9.9/12.7/13.5
1.96	11.6/11.7/11.5/11.6	3.4/6.8/11.2/19.5	8.0/8.1/8.9/11.1	2.3/4.6/7.1/13.1	2.6/2.5/2.5/2.6	13.2/17.5/24.4/27.5	9.3/9.4/9.5/10.7	5.3/7.4/10.3/11.2
2.06	12.6/12.7/12.5/12.6	3.8/5.2/6.8/10.4	7.9/8.0/8.1/8.3	2.3/3.2/4.3/6.4	2.8/2.7/2.7/2.8	9.0/13.7/21.2/25.7	9.7/9.9/10.1/10.4	3.3/5.3/8.1/9.6
2.16	13.6/13.7/13.5/13.6	3.8/5.0/6.2/7.8	7.8/8.1/8.2/8.4	2.2/2.8/3.6/4.5	3.1/3.0/3.0/3.0	11.7/21.3/29.8/36.1	10.4/11.4/11.6/12.0	4.0/7.7/10.5/12.6
2.26	14.5/14.6/14.4/14.5	3.3/4.6/5.7/7.2	7.9/8.1/8.6/10.8	1.8/2.4/3.1/3.9	3.3/3.1/3.2/3.2	39.1/52.9/64.9/76.7	10.0/10.3/10.7/12.8	12.5/17.9/21.6/25.4
2.36	15.4/15.5/15.3/15.4	3.8/5.2/6.1/7.5	7.9/9.2/9.5/12.9	1.9/2.6/3.1/3.8	3.5/3.3/3.4/3.4	30.2/54.9/84.4/96.7	13.0/14.3/15.2/16.2	9.0/17.3/26.2/30.2
2.46	16.2/16.3/16.1/16.2	5.7/6.4/7.3/8.3	8.2/8.5/8.6/8.7	2.7/3.1/3.5/4.0	3.7/3.5/3.6/3.6	32.4/55.7/86.8/100.9	15.0/15.3/17.3/18.0	9.1/16.5/25.5/29.6

- [3] S. K. Choi *et al.* (Belle Collaboration), Phys. Rev. Lett. **91**, 262001 (2003).
[4] M. Ablikim *et al.* (BESIII Collaboration), Phys. Rev. Lett. **110**, 252001 (2013).
[5] Z. Liu *et al.* (Belle Collaboration), Phys. Rev. Lett. **110**, 252002 (2013).
[6] K. Abe *et al.* (Belle Collaboration), Phys. Rev. Lett. **98**, 082001 (2007).
[7] B. Aubert *et al.* (BABAR Collaboration), Phys. Rev. Lett. **95**, 142001 (2005).

- [8] T. E. Coan *et al.* (CLEO Collaboration), Phys. Rev. Lett. **96**, 162003 (2006).
- [9] S. K. Choi *et al.* (Belle Collaboration), Phys. Rev. Lett. **100**, 142001 (2008).
- [10] A. Bondar *et al.* (Belle Collaboration), Phys. Rev. Lett. **108**, 122001 (2012).
- [11] B. Aubert *et al.* (BABAR Collaboration), Phys. Rev. Lett. **99**, 251801 (2007).
- [12] M. Gaspero (BABAR Collaboration), AIP Conf. Proc. 1257, 242 (2010).
- [13] C. Patrignani *et al.* (Particle Data Group), Chin. Phys. C **40**, 100001 (2016) and 2017 update.
- [14] E. Klempt and A. Zaitsev, Phys. Rept. **454**, 1 (2007).
- [15] M. Gronau and J. L. Rosner, Phys. Rev. D **92**, 114018 (2015).
- [16] Z. R. Huang, W. Chen, T. G. Steele, Z. F. Zhang and H. Y. Jin, Phys. Rev. D **95**, 076017 (2017).
- [17] S. Jia *et al.* (Belle Collaboration), Phys. Rev. D **95**, 012001 (2017).
- [18] C. F. Qiao and L. Tang, Phys. Rev. Lett. **113**, 221601 (2014); A. Pimikov, H. J. Lee, N. Kochelev, and P. M. Zhang, Phys. Rev. D **95**, 071501 (2017); A. Pimikov, H. J. Lee, and N. Kochelev, Phys. Rev. Lett. **119**, 079101 (2017).
- [19] L. Bellantuono, P. Colangelo and F. Giannuzzi, J. High Energy Phys. **1510**, 137 (2015).
- [20] C. P. Shen *et al.* (Belle Collaboration), Phys. Rev. D **88**, 011102(R) (2013).
- [21] A. Abashian *et al.* (Belle Collaboration), Nucl. Instr. and Methods Phys. Res. Sect. A **479**, 117 (2002).
- [22] J. Brodzicka *et al.*, Prog. Theor. Exp. Phys. (2012) 04D001.
- [23] S. Kurokawa and E. Kikutani, Nucl. Instr. and Methods Phys. Res. Sect. A **499**, 1 (2003), and other papers included in this volume.
- [24] T. Abe *et al.*, Prog. Theor. Exp. Phys. (2013) 03A001 and following articles up to 03A011.
- [25] D. J. Lange, Nucl. Instr. and Methods Phys. Res. Sect. A **462**, 152 (2001).
- [26] R. Brun *et al.*, GEANT, CERN Report No. DD/EE/84-1 (1984).
- [27] K. W. Edwards *et al.* (CLEO Collaboration), Phys. Rev. D **59**, 032003 (1999).
- [28] T. Sjöstrand, S. Mrenna and P. Skands, J. High Energy Phys. **05**, 026 (2006).
- [29] The Novosibirsk function is defined as $f(x) = \exp[-\frac{1}{2}(\ln^2(1 + \Lambda(x - x_0))/\tau^2 + \tau^2)]$ with $\Lambda = \sinh(\tau\sqrt{\ln 4})/(\sigma\sqrt{\ln 4})$. The parameters represent the mean (x_0), the width (σ) and the tail asymmetry (τ).
- [30] G. J. Feldman and R. D. Cousins, Phys. Rev. D **57**, 3873 (1998).
- [31] J. Conrad, O. Botner, A. Hallgren and C. Perez de los Heros, Phys. Rev. D **67**, 012002 (2003).